EXPERIMENTAL INVESTIGATION OF TURBULENT STRUCTURES OF FLOW AROUND A SPHERE

by

Vukman BAKIĆ, Martin SCHMID, and Branislav STANKOVIĆ

This paper presents the experimental investigation of turbulent structures of flow around a sphere. The mean velocity field and the turbulence quantities are obtained in a small low speed wind tunnel using, laser-Doppler anemometry, for the flow around a sphere at subcritical Reynolds number of 50,000. The results of laser-Doppler measurements are compared with results obtained by large eddy simulation. In this paper also flow visualization around sphere in the bigger wind tunnel and water channel for Reynolds numbers between 22,000 and 400,000 have been done.

Key words: *sphere, turbulent flow, flow visualization, laser-Doppler measurements, large eddy simulation*

Introduction

Many bodies of practical interest are bluff, and there are lots of studies which deal with various aspects of the complex flow around them. The basic structure of the flow past a sphere has been experimentally investigated using a variety of approaches, including flow visualization [1-6]. The primary interest in these investigations included visualization of the main vortex structure in the wake, understanding the vortex shedding mechanisms, measurement of frequencies present in the wake and of some integral parameters such as the streamwise drag and distribution of the mean pressure around the sphere.

Different flow regimes were determined experimentally: (1) the flow is laminar, and separation does not occur when the Reynolds number is lower than about 20, (2) separation occurs at Re 24 and results in the generation of an axis symmetric rings which is stable for Reynolds number up to Re = 210 when the wake becomes non axis symmetric, (3) at Re = 270 wake becomes unstable, and vortex loops began to shed from the sphere, and (4) when the Reynolds number is further increased to around 800, the vortex loops diffuse very rapidly, and the wake flow becomes turbulent. The turbulent range can be subdivided into four regimes: (a) sub critical regime up to Re 330,000 where there is a laminar boundary layer separation occurs at about $\alpha_s = 81°$ and position of separation remains almost unaltered over the range 10^4 Re $3.0·10^5$ followed by transition to fully turbulent flow downstream [6-7], (b) critical regime for Reynolds number between 300,000 and 330,000 which is characterized by a significant drop of the drag coefficient,

(c) supercritical regime between Re $3.3 \cdot 10^5$ to Re $2 \cdot 10^7$, and (d) transcritical regime for higher Reynolds numbers. Detailed experimental data on the mean flow structure and the structure of the turbulence are rare.

The use of surface roughness to trigger transition of the boundary layer is a common feature of many experiments. This technique is used not only for airfoil surfaces, but also for all types of body shapes and for applications wider than just in aeronautics. First well-known experiments with sphere and trip-wire have been done by Wiselberger (1914) [8]. He analyzed the drag coefficient and visualized the flow over a sphere with trip-wire. Fage (1929) [9] analyzed the effects of turbulence and surface roughness on the drag of a circular cylinder. He showed that the critical Reynolds number and drag coefficient decreased with increasing diameter of the trip-wire.

This experimental and numerical research is motivated by the absence of experimental data on the velocity field in the wake behind a sphere for high Reynolds numbers and by different sphere wake structure published by different authors. On the other hand, existing prediction methods – in particular those using Reynolds-averaged Navier-Stokes equations (RANSE) and turbulence models – fail to predict even integral quantities like drag, not to mention their inability to predict the wake characteristics [10]. These studies have also attempted to explain the mechanism through which the wake becomes unstable and to propose models for the vortex configuration in the sphere wake, using flow visualization technique.

Experimental apparatus and methods

The flow visualization has been carried out in a wind tunnel and in a water channel. The nozzle opening was 1.75   1.05 m. The working section is preceded by a 10:1 contraction with three turbulence-suppressing screens upstream of the contraction and 5.5 m long. The tunnel was operated in the range from $U_0 = 2$ m/s to 38 m/s. The turbulence level in the free stream was 0.89%. The sphere with $D = 0.165$ m in diameter was supported from the rear by a sting, which had a length $5D$ and a diameter $d = 0.12D$.

The dimension of the water-channel cross-section used in another set of visualization studies was 2.1   1.1 m. The sphere, with the same diameter as in the wind tunnel, was attached to a towing carriage and was supported from the rear by the same sting as in the wind tunnel. The blockage ratio was 1.15% for the wind tunnel and 0.8% for the water channel. The carriage was carefully designed to minimize mechanical vibrations when towed. The motion was initially accelerated and the sphere traveled a couple of meters before the final steady towing speed was reached. The range of speed of the carriage was $U_0 = 0.03$ to 2.3 m/s. The Reynolds number based on sphere diameter and velocity of air in the wind tunnel, or speed of towing carriage in water channel, could be varied from $2.2 \cdot 10^4$ to $4 \cdot 10^5$ in the wind tunnel and from $5 \cdot 10^3$ to $4 \cdot 10^5$ in the water channel.

Flow visualization in the big wind tunnel has been conducted by injecting smoke in the separation zone through holes in the supporting sting. The smoke particles were illuminated by a thin sheet of light created with a coherent laser beam and a cylindrical lens. The light source was a 10 W argon-ion laser operated in the multi-line mode, under which the smoke particles had a bright green color.

In the water channel dye was introduced into the boundary layer through holes with a diameter $d_h = 0.8$ mm at two locations at the sphere positioned at angles 45° and 135°, measured from the front stagnation point. Images of the smoke traces and dye were recorded with a MotionBlitz digital high-speed camera (500 frames/s) with a resolution of 256 228 pixels. Up to 2964 frames could be continuously recorded (6 seconds of real time). Digital images (bitmap-files) can be processed to produce animation in various formats (avi, mpg *etc*.). Digital color photographs with a resolution of 1024 768 pixels have also been taken, as well as color VHS videos at 50 frames/s.

The experiment of velocity measurements was performed in a small low speed wind tunnel. This tunnel has a contraction ratio of 1:4 and a test section with a square cross-section 300 mm wide, 300 mm high, and 600 mm long, with three turbulence suppressing screens upstream of the contraction. The tunnel operated with a wind speed of $U_0 = 12.6$ m/s. At this speed the free stream turbulence level, measured with hot wire anemometry (HWA), was 0.56%. A sphere with diameter $D = 61.4$ mm was supported from the rear by a sting which had a length $5.7D$ and a diameter $d = 0.13D$. The blockage ratio was 3.2%. The Reynolds number based on sphere diameter and velocity of air U_0 was Re = 51,500.

Velocity measurements have been carried out using two component forward laser-Doppler system manufactured by TSI. The 514.5 and 488 nm laser beams of an argon-ion laser were used to measure axial and radial components of velocity, respectively. The optics to focus the laser beams consist of a fiber measuring probe and transmitting lens with a focal length of $f = 350$ mm. The distance between the laser beams at the transmitting lens was 50 mm. With this optical arrangement the dimension of the measuring volume was 0.091 0.091 1.279 mm.

In the present experiments the air was seeded with water drops of the size of about 0.6-3 m. They were injected in the tunnel at the end of test section. A small amount of glycerol added to the water prevented the water from evaporating and helped the drops to maintain their size. Frequency analysis of the governing equation of motion of the water drops illustrated that the drops could faithfully follow sinusoidal motions with frequencies up to 10 kHz. The selected maximum frequencies are typical for the maximum energy – containing frequencies in turbulent air flows. The signals were processed using a TSI, model IFA-750, signal processor in coincidence mode. Coincidence windows between 20-100 s were used to get the Reynolds stresses.

Velocity field and turbulence characteristics of the flow around the sphere

The general character of sub-critical flow over a sphere is well understood. A laminar boundary layer forms on the upstream surface of the sphere. The flow accelerates as it is deflected by the sphere causing a sharp drop in pressure in stream-wise direction. For a Reynolds number of 51,500, the separation of laminar boundary layer happens at an angle between 80° and 83°. Behind the sphere a recirculation zone is formed, whose length is about $x/D = 1.5$ from the center of the sphere. The recirculation zone can be seen

in fig. 1 which shows contours of the axial mean velocity component U/U_0. The averaged axial velocity mean component has maximum values $U_{max} = 1.19U_0$ at the top of the sphere and the maximum reverse velocity is $U_{min} = -0.427\ U_0$. Figure 2 shows contours of radial mean velocity component V/U_0. The V component is positive in the region around the sphere and up to $x/D = 0.8$ with maximum values of $V/U_0 = 0.21$. The minimum value $V/U_0 = -0.11$ is found near re-attachment point.
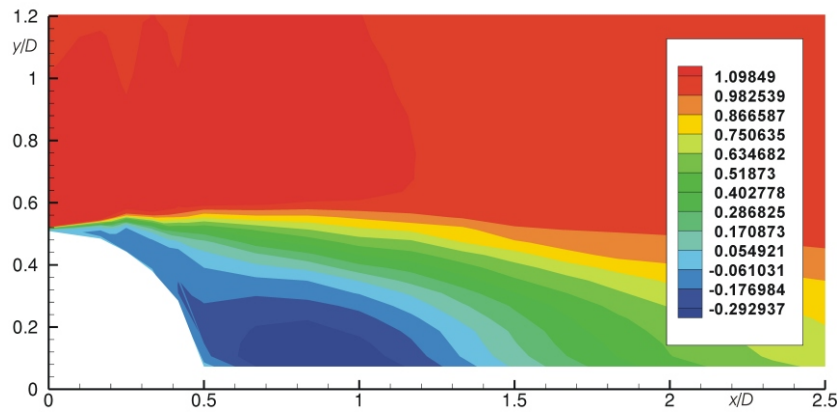

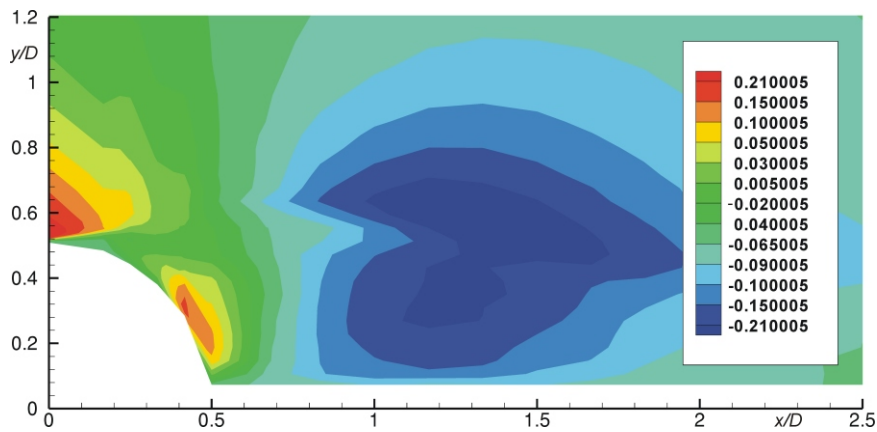**Figure 1. Contours of the measured axial mean velocity component U/U_0**

Figure 2. Contours of the measured radial mean velocity component V/U_0

Figure 3. and fig. 4 show the turbulence intensity in the axial and radial directions $(\overline{u^2})^{1/2}/U_0$ and $(\overline{v^2})^{1/2}/U_0$, respectively, while fig. 5 shows the Reynolds stress $\overline{uv}/U_0^2$.
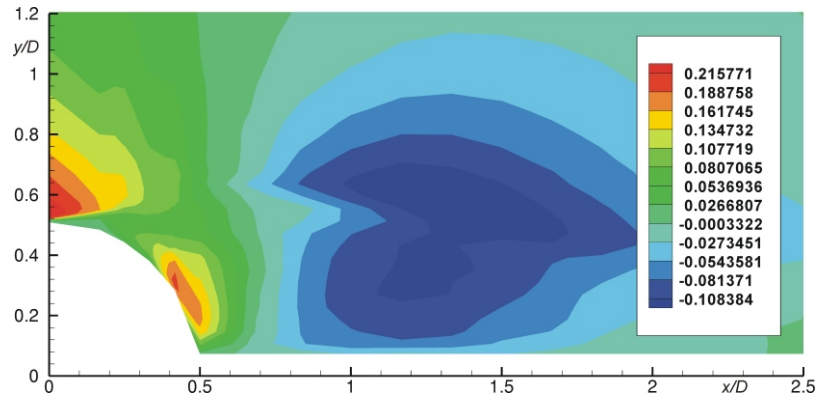
100

Figure 3. Contours of the measured turbulent intensity in axial direction $(\overline{u^2})^{1/2}/\ U_0$
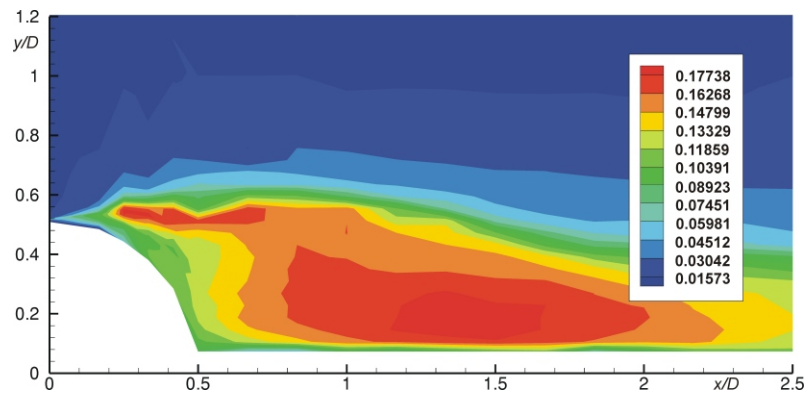

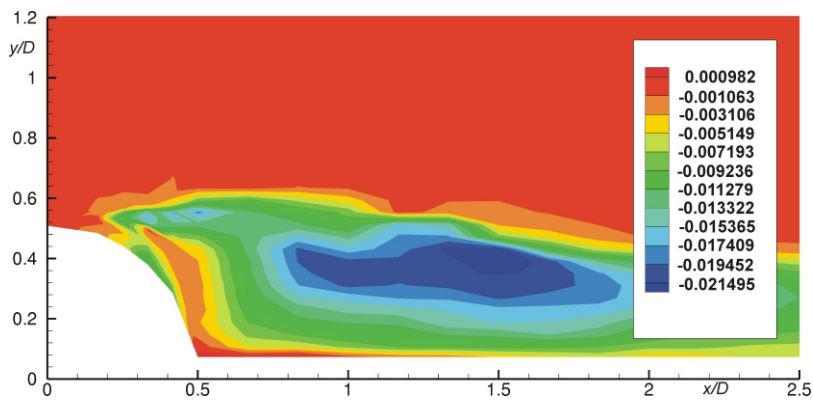**Figure 4. Contours of the measured turbulent intensity in radial direction**

Figure 5. Contours of the measured Reynolds stress

The turbulence intensity in axial direction $(\overline{u^2})^{1/2}/U_0$ is the largest with maximum values in the shear layer. Experimental investigation done in [11] showed that the maximum of axial turbulence intensity $(\overline{u^2})^{1/2}/U_0$ is found behind the sphere ($x/D > 0.5$), but this measurements and the large eddy simulation (LES) done by Schmid (2001) [12] show that maximum of this turbulence intensity lies actually almost at the beginning of the free shear layer development. The width of the shear layer after separation is small and increase due to roll-up off the eddies. Direct numerical simulation (DNS) of the flow around the sphere at Re = 5,000 [13] showed (with the help of invariant map) that the state of turbulence in the shear layer shortly after separation is nearly one-dimensional, with fluctuations primarily in stream-wise direction. After roll-up and brake-down of vortex ring, the turbulence becomes three-dimensional and attains a nearly isotropic state in the re-attachment zone. The value of the turbulence intensity in radial direction $(\overline{v^2})^{1/2}/U_0$ increased slowly in the shear layer and overtook the maximum at the end of the recirculation zone. The Reynolds stress $\overline{uv}/U_0^2$ is positive before transition and than becomes negative in the wake of the sphere.

Comparison of experimental results with numerical results

Numerical studies of the flow around a sphere at high Reynolds number are rare. Jonson and Patel [14] and Tomboulides and Orszag [15] predicted laminar flow. Tomboulides, Orszag, and Karniakidis [16] perfomed LES for Re = 20,000 using a sub-grid turbulence model based on normalization group theory. Constantinescu and Squires [17] performed LES and the detached eddy simulation (DES) for Re = 10,000.

A comparison of the experimental data with LES, figs. 6 and 7 show, overall, a good agreement contrary to RANSE calculations. The LES has been performed under slightly different conditions than the experiment. The sting in the LES had a diameter $d = 0.1D$, and the lateral boundary of the solution domain was $10D$ away from the sphere. In the experiment, $d = 0.13D$ has been used, and the sphere was mounted in the center of the channel whose width was less than $5D$. In the numerical simulation has tested different subgrid-scale models (Smagorinsky, dynamic and no model) and has found that for the Reynolds number 50,000 the subgrid-scale model plays a minor role. The results depended much more on grid quality. A local grid refinement used in critical regions like the separation point and the shear layer. The grid is refined locally at the surface of the sphere, along the stick and in regions of large variable changes, as indicated by previous test simulations. For the simulation, also, the Smagorinsky model without damping function was used. It was developed and has been tested for channel flows with good results, but is considered not suitable for this case, because the transition takes place in the free shear layer and not wall-initiated. In separated turbulent flows the law of the wall generally is not valid and it has not been shown so far that the damping function is correct for this type of flows. Therefore no wall functions were used here but very fine grid in the normal direction has been generated near the wall in order to resolve the boundary layer. The first computational point next to the wall lies always at a normalized distance $y^+< 1$.

102

The coarser numerical mesh contains 840,000 CVs and is locally refined to resolve the boundary layer and to save memory and computing time in regions where the flow is unaffected by the body. A finer grid has a similar structure but is further locally refined and has around $1.9 \cdot 10^6$ CVs.

A large amount of CPU time was spent to optimize the grid, because the computation of 1000 time steps at least was necessary for each test simulation. For the time averaged results time integration was carried out over 30,000 time steps (particles in the flow would pass within this time through a domain of the size of sphere more than 300 times). Second order discretization methods are used (midpoint rule integral approximation, linear interpolation and central differences), except in regions far from the sphere

Figure 6. Comparison of radial (right) and axial (left) velocity components obtained by LES and in experiments

and wake, where a small portion of a first order upwind approximation is blended with the second order approximation in order to avoid oscillations on a coarse grid (there is no turbulence there and the flow is basically potential).

The method of domain decomposition is used for parallelization: the model is subdivided into pieces of equal size, and the variables are exchanged across interfaces after each iteration. The efficiency of parallelization, depends upon the problem size and number of used processors: for the simulation of the flow around the sphere 64 processors on CRAY T3E have been used. For the same number of processors the total efficiency was determined around 90%.

Figure 6 shows a comparison of mean axial and radial velocity components obtained in the present experiment and in the LES. The agreement of axial velocity is very
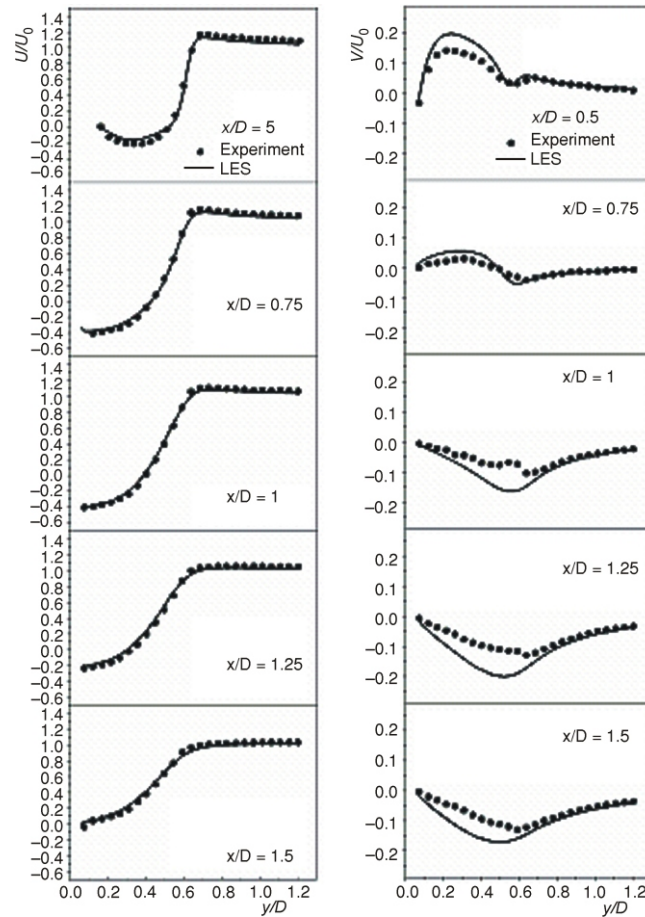
good. The length of the recirculation region predicted by LES is $L = 1.5D$, which is in agreement with the length of recirculation region obtained in experiments. The separation point predicted by LES is 84° from front stagnation point. In the experiments the separation point is at 82° from the front stagnation point. Profiles of radial components show only qualitatively good agreement between LES and experiments. The difference is probably due to the different size of the flow domain, since in LES the lateral walls which constrained the flow were not present and the sting was thinner. The turbulence intensity and Reynolds stresses, fig. 7, also show qualitatively good agreement between LES and experiments.
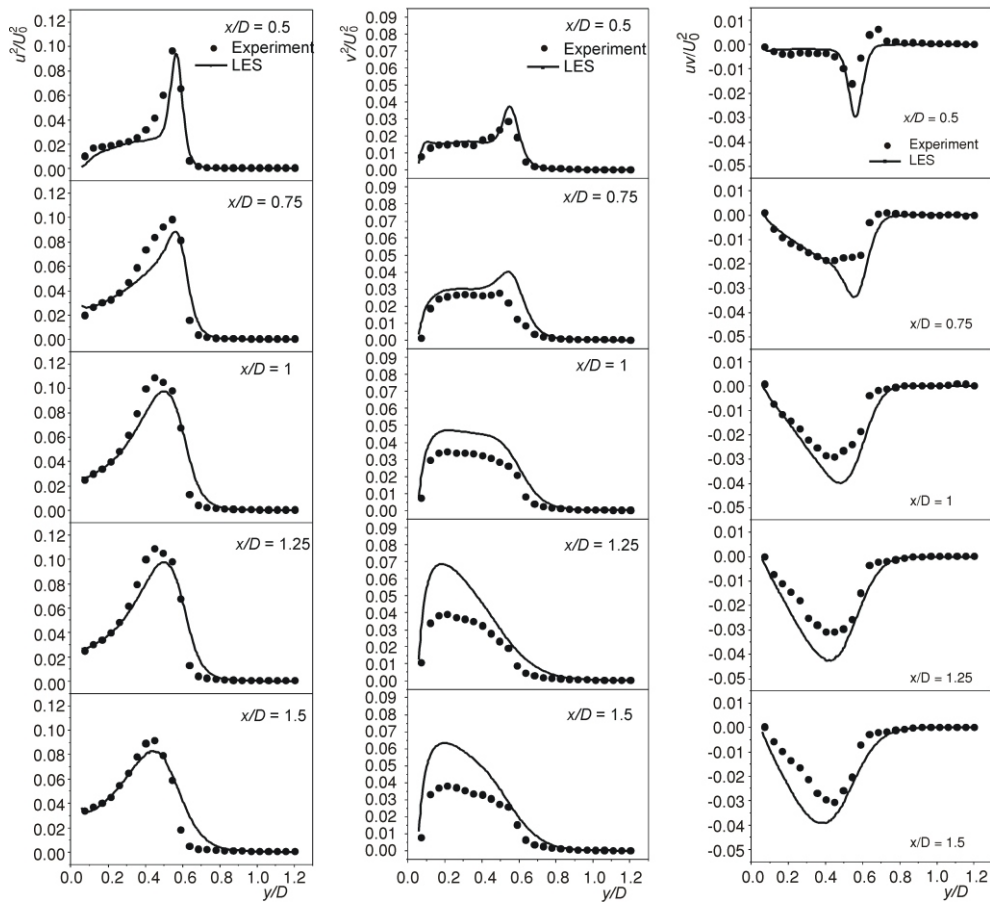

Figure 7. Comparison of Reynolds stresses components obtained by LES and in experiments

Flow visualization in the wind tunnel and
in the water channel

The smoke particles were illuminated in a thin laser light sheet which could be positioned in the (x, y), (x, z) or (y, z) plane, x being in the flow direction. Figure 8 shows visualization of the flow around sphere in the wind tunnel in the (x, y) plane for Reynolds numbers 22,000 and 50,000. The observed near-wake recirculating region is large and the wake performs a progressive wave motion. At the lower Reynolds number large coherent structures are clearly. The videos and the photographs show the roll-up of the sep-
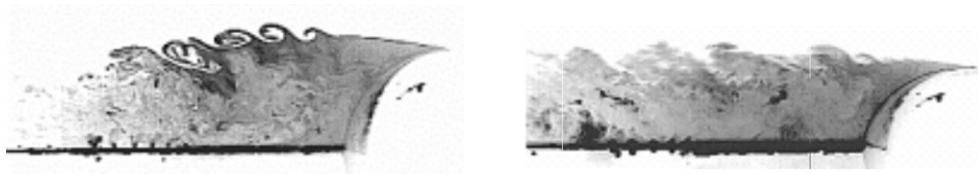

Figure 8. Visualization of flow around sphere using smoke in a wind tunnel for Re = 22,000 (left) and Re = 50,000 (right)

arated shear layer and pairing of vortices. The roll-up and the pairing processes can be more clearly observed in the water-channel visualization (fig. 11) for Reynolds numbers up to 175,000. At Reynolds number of 50,000, in the wind tunnel, the turbulence structure in the mixing layer is so fine that roll-up and pairing processes were not visible with the present camera allowing 500 frames/s.

In order to determine the three-dimensional structure of the wavy wake, the laser sheet was positioned in the plane normal to the flow direction, (y, z) plane, 5.5D downstream of the sphere. Figure 9 shows the characteristic changes of vortex patterns by the time for Re = 22,000. Achenbach [1] found, by analyzing hot wire signals, that the vortex separation points rotate around the sphere for Reynolds numbers above 6,000. This suggests a single helical wake configuration.

The existence of a helical vortex system does not respect Thomson's circulation theorem. This theorem states that if the incident flow is free from vorticity, the net flux of the vorticity across planes perpendicular to the wake axis must be zero. This led Pao and Kao [18] to propose a complex double helix, which unwinds in the opposite sense. However from pictures in fig. 9 and from corresponding films, no regularity of rotation of vortices could be observed, and also for Re = 50,000 [19]. The wake is not completely filled by smoke since it was introduced through holes at the upper and lower side of the sting. The visible smoke in the wake cross-section shown in fig. 9 changes its shape and moves left-right and up-down, but no regularity could be identified in this motion over the continuous recording of 6.2 s of real time.
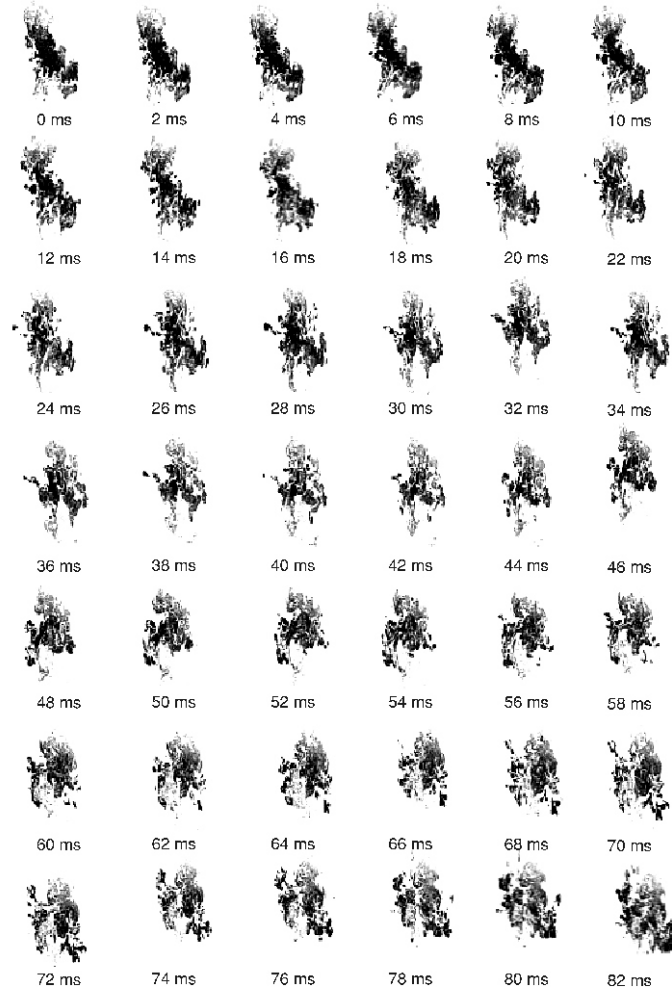
Figure 9. Structure of the sphere wake in a plane normal to the wake axis 5.5D downstream from sphere, and for Re = 22,000

With the Reynolds numbers increasing from sub-critical 22,000 to critical 350,000, the point of boundary layer separation moves from about 82° to 132°. At the same time the position of transition moves towards the sphere and the rate of entrainment tends to increase. Once the transition point comes close enough to the sphere wall as the Reynolds number is increased, it causes the boundary layer to become turbulent further downstream; thus, laminar separation is often followed by turbulent re-attachment after a short distance, with turbulent boundary layer remaining attached before it separates again further downstream. Hence, the near-wake recirculating region shrinks suddenly and the wavy motion of the wake vanishes. The vanishing of progressive wavy motion of the
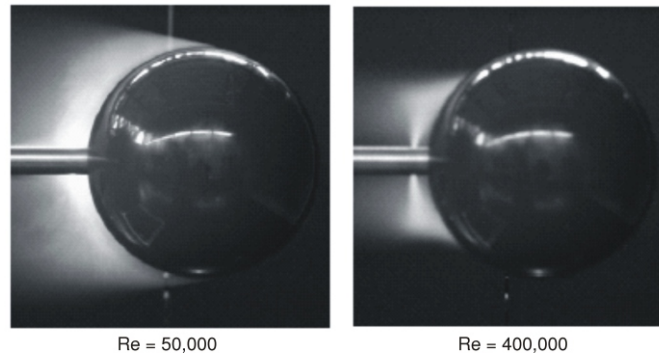
106

Figure 10. Long exposure visualization of the flow around sphere for Re = 50,000 and Re = 400,000

wake behind the sphere is obvious at Reynolds number $4 \cdot 10^5$. The transition to turbulence in the boundary layer substantially decreases the wake size, as can be seen in fig. 10.

The characteristics of boundary layer separation and laminar turbulent transition have also been investigated in a water channel at Reynolds numbers from 5,000 to 380,000. The boundary layer was colored by dye. Due to the difference in kinematics viscosity, the same Reynolds number is achieved at lower velocity than in air, allowing a better time resolution with the camera at 500 frames/s. The separation, laminar-turbulent transition and growth of a separated shear layer depend on many factors and were subject of many experimental and theoretical investigations. Figure 11 shows these processes for
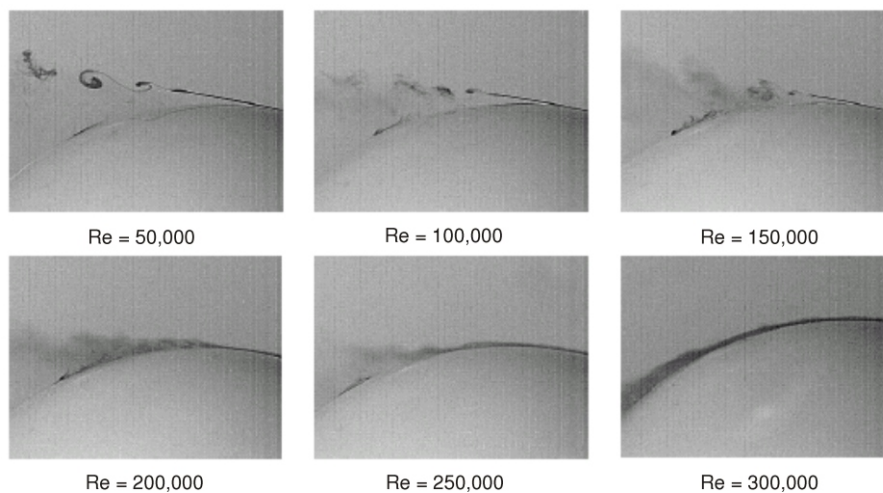

Figure 11. Separation and transition of a boundary layer over sphere for different Reynolds numbers

different Reynolds numbers separated shear layer depend on many factors and were subject of many experimental and theoretical investigations. The shear layer formed after the separation of boundary layer is subjected to Kelvin-Helmholtz instability, which causes the roll-up of vortex rings at nearly regular time intervals. It appears that for all cases with laminar separation, the first two vortex rings seen are laminar; the third one is already turbulent and further downstream no regular structure can be observed any more. From these pictures and corresponding film, it is obvious that, with increasing Reynolds number, the turbulence structures in the mixing layer become finer and transition of the separated shear layer occurs closer to the separation point. For Re = 250,000, the movie shows that at the separation point the boundary layer is not completely laminar. There are intervals of time when the boundary layer is turbulent and separation occurs later. At the critical Reynolds number around Re 300,000, the transition from laminar to turbulent boundary layer occurs before separation and the turbulent boundary layer separates much later, at an angle close to 135°. It appears that, after becoming turbulent, the rolled-up vortices start interacting with the wall when the Reynolds number is high enough so that the transition happens close to the separation point. This can be observed from Re = 200,000 onwards; this causes the separated boundary layer to re-attach and become separated further downstream.

Figure 12 shows that besides the roll-up of vortices, pairing of vortices is also present in the free shear layer of a sphere. The roll-up includes the folding, rolling and break-up of a continuous vortex sheet into discrete vortices, while pairing means a sequential amalgamation of these vortices into larger vortex structures. If experiment is carefully controlled and prepared it, is possible to see that more than two vortices combine to form still larger vortices [20]. The roll-up process of a shear layer occurs at a loca-
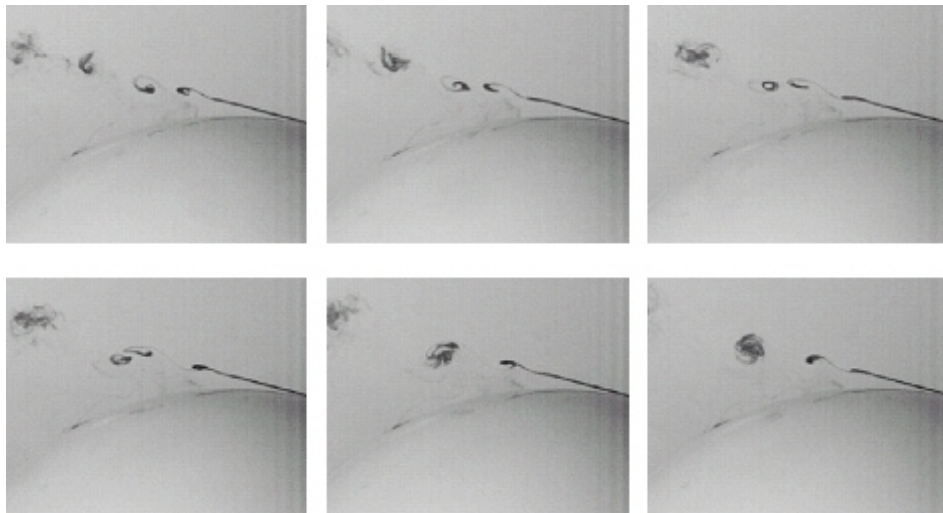

Figure 12. The process of vortex pairing at Re = 50,000

108

tion at which the fundamental frequency (natural instability frequency) attains its maximum amplitude and is followed by the generation of a sub-harmonic frequency, as described in [21]. The roll-up and pairing of vortices observed here is similar to the processes found in mixing layers.

Successive amalgamation of pairs of neighboring vortices marked by dye is evident in fig. 12. During the pairing, vorticity is continuously being redistributed into larger and larger eddies, whose wavelength and size double at each interaction. Winant and Browand [22] have shown that merging of vortices was indeed the primary process governing the stream-wise growth of the mixing layer thickness. However, sub-harmonics alone can not explain the complicated nature of

Figure 13. Distribution of low-mode and high-mode Strouhal numbers as a function of Reynolds number

shear layer development. According to [23] the location at which pairing occurs coincides with the location at which the amplitude of the sub-harmonic mode frequency attains a maximum. The value of the natural instability frequency of the shear layer for different Reynolds numbers is obtained from the present experiments by counting roll-up of vortices with time in the high speed digital video. These results, together with results from other researchers are shown in fig. 13. This figure shows the distribution of low-mode and high-mode Strouhal number versus Reynolds number $St = fD/U_0$, where f is the frequency, D diameter of sphere, and U_0 the free-stream velocity.

Experimental investigations of frequencies in a sphere wake [2], obtained from spectra of velocity fluctuations detected by a hot-wire in unexcited flow, showed the presence of several dominant frequencies: low frequency, a higher frequency, and often the sub-harmonic of the higher frequency. The higher frequency (high-mode of Strouhal number), was detectable only in the region of the wake immediately downstream of the sphere, but low frequency (low-mode of Strouhal number) could be observed in a much larger region. The sub-harmonic of the higher frequency obtained in this experiment was produced by pairing of vortices, which is obvious from our flow visualization.

Kim's and Durbin's [2] data does not show a unique power-law dependence of frequency of the Kelvin-Helmholz shear layer instability f_{KH} on Reynolds number: for $10^3 < Re < 10^4$ frequency scales approximately with $Re^{0.75}$ while at higher Reynolds numbers the exponent is closer to 0.66. Our experiments, for Reynolds number $Re > 22,000$, give a power law:

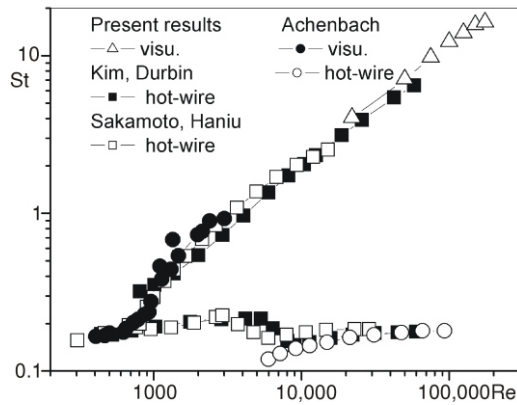$$St = 0.0039Re^{0.695} \qquad (1)$$

This result is in good agreement with Kelvin-Helmholtz frequency of shear layer instability for the flow around a circular cylinder obtained in [24]. This frequency is usually normalized by the shedding or Karman frequency f_K of the large vortices in the wake. Prasad and Williamson [24] found that the frequency scales for Re < 10^5 with power law:

$$\frac{f_{KH}}{f_K} \sim 0.0235\,\mathrm{Re}^{\,0.67} \tag{2}$$

where the exponent and the constant are found by analyzing experimental data. In [24], data analysis indicates a higher exponent for Re > 10^5:

$$\frac{f_{KH}}{f_K} \sim \mathrm{Re}^{\,0.7} \tag{3}$$

According to our flow visualization and an experimental investigation by Kim and Durbin [2] we can conclude that the measured higher frequency, high mode of Strouhal number, corresponds to the instability frequency of the shear layer. However, flow visualization showed no evidence of discrete vortex shedding behind the sphere; for that reason we can agree with [2] that the measured low frequency, the low mode of Strouhal numbers, corresponds to the large scale (sinus) instability of the sphere wake.

Conclusions

The turbulent flow around a sphere attached to a sting at the rear stagnation point was investigated experimentally using flow visualization technique and laser Doppler anemometry (LDA) in wind tunnel. Visualization experiment was carried out in a wind tunnel and in a water channel to determine the wake structure, separation and laminar-turbulent transition of a separated boundary layer behind a sphere. The range of Reynolds numbers covered varied from 22,000 to 400,000 in a wind tunnel and from 50,000 to 300,000 in a water channel. For flow visualization the smoke and dye methods were used.

The results of flow visualization indicated that the wake structure of a sphere, and the vortex configuration, is more complicated than the simple helical or double helical vortex structure that were reported in some earlier publications. Films and photographs showed the roll-up of the separated shear layer and the pairing of vortices, indicating that besides the natural instability frequency which defines the high-mode Strouhal number, there also exists a sub-harmonic of this frequency.

Experimental data obtained using LDA are compared with results obtained by LES. The LES is applied to a geometrically complex flow utilizing the advantages of advanced numerical CFD techniques such as local grid refinement. The Smagorinsky subgrid-scale model was used in a LES. LES and experimental results are in reasonable agreement.

110

Nomenclature

D — diameter of sphere, [mm]
d — diameter of sting, [mm]
d_h — diameter of holes, [mm]
f — focal length, [mm]
L — length of recirculation zone,
Re — Reynolds number ($= UD/\nu$), [–]
St — Strouhal number ($=fD/V_0$), [–]
U — mean axial velocity, [m/s]
U_0 — mean velocity in free stream, [m/s]
$(u^2)^{1/2}$ — axial root means square, [m/s]
$\underline{u_\tau}$ — velocity on the wall, [m/s]
$\overline{uv}$ — Reynolds shear stress, [m^2/s^2]
V — mean radial velocity, [m/s]
$(v^2)^{1/2}$ — radial root means square, [m/s]
x — axial distance from sphere center, [mm]
y — radial distance from sphere center, [mm]
y^+ — normalized distance [$= y(u_\tau/\nu)$], [–]

Greek letters

α_s — angle of separations, [°]
ν — kinematics viscosity, [m^2/s]

Acknowledgment

References

[1] Achenbach, E., Experiments on the Flow Past Spheres at Very High Reynolds Numbers, *Journal of Fluid Mechanics, 54* (1972), pp. 565-575
[2] Kim, H. J., Durbin, P. A., Observations of the Frequencies in a Sphere Wake and of Drag Increase by Acoustic Excitation, *Physics of Fluids, A 31* (1988), pp. 3260-3265
[3] Sakamoto, H., Haniu, H., A Study of Vortex Shedding from Sphere in a Uniform Flow, *Transactions of the ASME, 112* (1999), pp. 386-392
[4] Taneda, S., Visual Observations of the Flow Past a Sphere at Reynolds Numbers between 10^4 and 10^6, *Journal of Fluid Mechanics, 85* (1978), pp. 187-192
[5] Bakić, V., Experimental Investigation of a Flow Around a Sphere, *Thermal Science, 8* (2004) 1, pp. 63-81
[6] Magarvey, R. H., Bishop, L. R., Transition Ranges for Three-Dimensional Wakes, *Canadian Journal of Physic, 39* (1961), pp. 1418 – 1422
[7] Raithby, G. D., Eckert, E. R. G., The Effect of Support Position and Turbulence Intensity on the Flow Near the Surface of a Sphere, *Wärme und Stoff, 1* (1968), pp. 87-94
[8] Wieselberger, C., A Sphere Drag, *Zeitschrift für Mechanics, 5* (1914), pp. 140-144
[9] Fage, A., The Effects of Turbulence and Surface Roughness on the Drag of a Circular Cylinder, *Reports and Memoranda, 1283* (1923), pp. 248-255
[10] Hadžić, I., Bakić, V., Perić, M., Sajn, V., Kosel, F., Experimental and Numerical Studies of Flow Around Sphere at Subcritical Reynolds Number, *Proceedings ,* Engineering Turbulence Modeling and Experiments 5, Mallorca, Spain, 2002, pp. 667-675

[11] Leder, A., Geropp, D., The Unsteady Flow Structure in the Wake of the Sphere, in: Laser Anemometry Advances and Applications, 1993, pp. 119-125
[12] Schmid, M., Large Eddy Simulation of Turbulent Flow with Unstructured Grid and with Finite Volume Parallel Methods (in German), Ph. D. thesis, TUHH, Hamburg, Germany, 2001
[13] Seidl, V., Development and Use of Parallel Finite Volume Procedure for Flow Simulation Using Unstructured Grid with Local Refinement (in German), Ph. D. thesis, TUHH, Hamburg, Germany, 1997
[14] Johnson, T. A., Patel, V. C., Flow Past a Sphere Up to a Reynolds Number of 300, *Journal of Fluid Mechanics, 378* (1999), pp. 19-70
[15] Tomboulides, A. G., Orszag, S. A., Numerical Investigation of Transitional and Weak Turbulent Flow Past a Sphere, *Journal of Fluid Mechanics, 416* (2000), pp. 45-73
[16] Tomboulides, A. G., Orszag, S. A., Karniakidis, S. A., Direct and Large Eddy Simulations of Axis Symmetric Wakes, in: Engineering Modeling and Experiments 2 (Eds. W. Rodi F. Martelli), 1993, pp. 273-282
[17] Constantinescu, G. S., Squires, K. D., LES and DES Investigations of Turbulent Flow Over a Sphere at Re = 10,000, *Flow, Turbulence and Combustion, 70* (2003), pp. 267-298
[18] Pao, H. P., Kao, T. W., Vortex Structure in the Wake of a Sphere, *Physics of Fluids, 20* (1977) 2, pp. 187-191
[19] Bakić, V., Experimental Investigation of Turbulent Flows Around a Sphere, Ph. D. thesis, TUHH, Hamburg, Germany, 2003
[20] Ferziger, J. H., Direct and Large Eddy Simulation of Turbulence, Lecture note: Understanding, Modelling and Simulation of Turbulence, Hamburg, Germany, 1999
[21] Ho, C. M., Huerre, P., Perturbed Free Shear Layers, *Annual Revue of Fluid Mechanics, 16* (1984), pp. 365-424
[22] Winant, C. D., Browand, F. K., Vortex Pairing, the Mechanism of Turbulent Mixing-Layer Growth at Moderate Reynolds Numbers, *Journal of Fluid Mechanics, 63* (1974), pp. 237-255
[23] Ho, C. M., Huang, L. S., Subharmonics and Vortex Merging in Mixing Layers, *Journal of Fluid Mechanics, 119* (1982), pp. 443-473
[24] Prasad, A., Williamson, H. K., The Instability of the Shear Layer Separating from a Bluff Body, *Journal of Fluid Mechanics, 333* (1997), pp. 375-402

V. Bakić
VINČA Institute of Nuclear Sciences
Laboratory for Thermal Engineering and Energy
P. O. Box 522, 11001 Belgrade, Serbia and Montenegro

M. Schmid
c.a.r.u.s. Information Technology AG
Bornbarch 9
22848 Norderstedt, Germany

Coresponding author (V. Bakić):
E-mail: bakicv@vin.bg.ac.yu

112